PIP_2 regulation of TRPC5 channel activation and desensitization

Received for publication, January 24, 2021, and in revised form, April 20, 2021 Published, Papers in Press, April 30, 2021,
https://doi.org/10.1016/j.jbc.2021.100726

Mehek Ningoo[1], **Leigh D. Plant**[1,2], **Anna Greka**[3,4], **and Diomedes E. Logothetis**[1,2,5,*]

From the [1]*Department of Pharmaceutical Sciences, School of Pharmacy, Bouvé College of Health Sciences,* [2]*Center for Drug Discovery, Northeastern University, Boston, Massachusetts, USA;* [3]*Department of Medicine, Brigham and Women's Hospital and Harvard Medical School, Boston, Massachusetts, USA;* [4]*Broad Institute of MIT and Harvard, Cambridge, Massachusetts, USA;* [5]*Department of Chemistry and Chemical Biology, College of Science, Northeastern University, Boston, Massachusetts, USA*

Edited by Mike Shipston

Transient receptor potential canonical type 5 (TRPC5) ion channels are expressed in the brain and kidney and have been identified as promising therapeutic targets whose selective inhibition can protect against diseases driven by a leaky kidney filter, such as focal segmental glomerular sclerosis. TRPC5 channels are activated not only by elevated levels of extracellular Ca^{2+}or lanthanide ions but also by G protein ($G_{q/11}$) stimulation. Phosphatidylinositol 4,5-bisphosphate (PIP_2) hydrolysis by phospholipase C enzymes leads to PKC-mediated phosphorylation of TRPC5 channels and their subsequent desensitization. However, the roles of PIP_2 in activation and maintenance of TRPC5 channel activity *via* its hydrolysis product diacyl glycerol (DAG), as well as the mechanism of desensitization of TRPC5 activity by DAG-stimulated PKC activity, remain unclear. Here, we designed experiments to distinguish between the processes underlying channel activation and inhibition. Employing whole-cell patch-clamp, we used an optogenetic tool to dephosphorylate PIP_2 and assess channel–PIP_2 interactions influenced by activators, such as DAG, or inhibitors, such as PKC phosphorylation. Using total internal reflection microscopy, we assessed channel cell surface density. We show that PIP_2 controls both the PKC-mediated inhibition and the DAG- and lanthanide-mediated activation of TRPC5 currents *via* control of gating rather than channel cell surface density. These mechanistic insights promise to aid in the development of more selective and precise inhibitors to block TRPC5 channel activity and illuminate new opportunities for targeted therapies for a group of chronic kidney diseases for which there is currently a great unmet need.

Transient receptor potential canonical type 5 (TRPC5) channels belong to the classical TRPC family of nonselective, calcium-permeable cation channels (1). They are widely expressed in many tissues, including the brain, where they are involved in fear-related behaviors, regulating hippocampal neurite length as well as growth cone morphology, and the kidney, where they are largely implicated in chronic kidney disease. In kidney podocytes, cells essential for the kidney filter, TRPC5 channels may be promising therapeutic targets because their selective inhibition is protective against diseases driven by a leaky kidney filter in rodents (2–6). Mammalian TRPC5 channels are transiently stimulated by the action of phospholipase C (PLC) enzymes, either GTP-binding protein–coupled receptors coupled to $G_{q/11}$ that signal through PLCβ_1 or tyrosine kinase–coupled receptors through PLCγ_2 (1–4). Activation of PLC causes the hydrolysis of plasma membrane phosphatidylinositol 4,5-bisphosphate (PIP_2) to form inositol 1,4,5-triphosphate (IP_3) that releases Ca^{2+} from intracellular stores and diacylglycerol (DAG) which activates PKC (1–7).

Since the mid-1990s, PI(4,5)P_2 (PIP_2) has been appreciated to act beyond its role as a precursor to the ubiquitous signaling of its products (*e.g.*, IP_3, DAG, PIP_3) as a direct regulator of membrane protein function, especially ion channel proteins (8, 9). Cocrystal structures of Kir channels with PIP_2 have revealed at atomic resolution specific residue interactions with the phosphates at positions 4' and 5' of the inositol ring of PI(4,5)P_2 around the two channel gates of Kir channels (10–12). Microsecond-long molecular dynamics simulations have revealed how gating molecules, such as the Gβγ subunits or Na^+, open one, the other, or both gates of Kir3 channels by enhancing specific residue interactions with PIP_2 (13). The relationship of TRPC5 with PIP_2 has not yet been structurally elucidated (14).

TRPC5 channels can also be steadily activated by elevated levels of extracellular Ca^{2+} or application of lanthanide ions, such as lanthanum (La^{3+}) and gadolinium (Gd^{3+}) (15, 16). These cations bind to an extracellular cation-binding site located in the vicinity of the channel's pore entrance (15, 16). The extracellular cation-binding site consists of two acidic Glu residues, E543 and E595, mutation of either of which to Gln renders TRPC5 lanthanide insensitive. The Gln mutant channels can still be activated through PLC stimulation, suggesting that the two mechanisms of channel activation are independent (17).

Although it had been thought that the PIP_2 hydrolysis products IP_3 and DAG do not themselves activate TRPC5 channels, evidence for a mechanism that renders the channel

* For correspondence: Diomedes E. Logothetis, d.logothetis@northeastern.edu.
Present address for Mehek Ningoo: Graduate School of Biomedical Sciences, Icahn School of Medicine at Mount Sinai, New York, NY 10029, USA.

sensitive to DAG-mediated activation has been presented (2). This mechanism requires Gq receptor–mediated activation of PLC and hydrolysis of PIP_2, causing a conformational change in the C terminus of TRPC5 that leads to dissociation of the Na^+/H^+ exchanger regulatory factor (NHERF) protein from a PDZ-binding motif (2). NHERF proteins serve to link integral membrane proteins to the cytoskeleton, and NHERF dissociation allows the channel to be activated by DAG (2).

TRPC5 channels that are dependent on PLCβ or PLCγ activation exhibit current desensitization by a mechanism attributed to PKC-mediated phosphorylation (18, 19). In this scheme, DAG-mediated activation of TRPC5 channels precedes activation of PKC which phosphorylates the channel at T972 to cause desensitization by an unknown mechanism (19). PKC phosphorylation of the channel at T972 has been proposed to increase the affinity of the C terminus of the channel to bind to NHERF1, blocking activation by DAG (2). Mutating the Thr residue to Ala (T972A) protects the channels from being phosphorylated by PKC and prevents desensitization (2), favoring DAG over NHERF binding to result in channel activation. For G protein–gated Kir3 channels, PKC-mediated channel phosphorylation has been shown to weaken channel-PIP_2 interactions and, together with PIP_2 hydrolysis, to underlie current desensitization (20, 21). To date, although PIP_2 regulation of TRP channels is being widely studied (18, 19, 22), the roles of PIP_2 in maintaining TRPC5 channel activity and its involvement in the DAG-mediated stimulation and PKC-mediated desensitization of activity remain unclear.

The present work provides evidence that trivalent cation and PLC-mediated activation of TRPC5 allosterically and independently converge on PIP_2 to gate the channel. Both the PKC-mediated phosphorylation of T972 and direct PIP_2 depletion contribute to TRPC5 current inhibition. PKC phosphorylation of the channel weakens channel–PIP_2 interactions, whereas DAG-mediated activation of the PKC-insensitive T972A mutant strengthens channel–PIP_2 interactions. Our findings support a paradigm whereby PIP_2 hydrolysis and DAG generation play a dual role in $G_{q/11}$ protein–mediated TRPC5 channel activation. First, in the absence of phosphorylation at T972, DAG is able to strengthen channel–PIP_2 interactions and stimulate activity. Second, DAG activates PKC that in turn phosphorylates the channel at T972, driving activity toward full inhibition by weakening channel–PIP_2 interactions and enabling loss of PIP_2 from the channel, given the surrounding depleted levels.

Results

Gq-mediated inhibition of TRPC5 currents is dependent on PIP_2

Activation of Gq signaling evokes a transient TRPC5 current that subsequently decreases in magnitude *via* a mechanism that is proposed to require phosphorylation of the channel at threonine 972 by PKC (18). To determine if the PKC-mediated decrease in TRPC5 currents is PIP_2 sensitive, we used whole-cell patch clamp recording to study HEK293T cells transiently expressing mTRPC5–GFP under experimental conditions where PIP_2 levels were elevated or lowered. Double-rectifying TRPC5 currents were elicited by voltage ramps from −100 mV to +100 mV after application of 100 μM carbachol (CCh), an agonist at the Gq-coupled muscarinic type 3 receptors that are endogenously expressed in HEK293T cells (Fig. 1*A*) (23). After the initial activation of the channel, TRPC5 currents spontaneously decreased in magnitude, as expected (Fig. 1*A*-top). To probe if the rate of PKC-mediated channel inhibition is PIP_2 sensitive, we increased the level of PIP_2 in the HEK293 cells through two types of manipulations: First, we increased production of PIP_2 by cotransfecting mTRPC5–GFP with phosphatidylinositol 4-phosphate 5 kinase (PIP-5K), the enzyme that phosphorylates PI(4)P at position 5' of the inositol ring (Fig. 1*A*-middle). Second, we increased PIP_2 levels directly by including 200 μM dioctanoylglycerol-PIP_2 (diC_8–PIP_2), a soluble analog of PIP_2 in the patch pipette, as before (24) (Fig. 1*A*-bottom). Both PIP-5K overexpression and inclusion of diC_8–PIP_2 in the patch pipette reduced the extent to which TRPC5 currents decreased after activation by CCh (Fig. 1, *A* and *B*). Next, we studied the effect of depleting intracellular PIP_2 levels by incubating the cells in 20 μM wortmannin, a fungal sterol that at micromolar concentrations inhibits both PI3K and PI4K, of which PI4K is required to generate PIP_2 (5). After a 1-h incubation with wortmannin, CCh-activated TRPC5 currents showed a higher rate of the spontaneous inhibition than untreated controls (Fig. 1*C*). Together, these findings indicate an inverse relationship between PIP_2 levels and PKC-induced inhibition of channel currents.

TRPC5 channels are also activated by extracellular trivalent lanthanide ions *via* a mechanism that is independent of Gq signaling, does not activate PKC-mediated phosphorylation, and is not associated with a subsequent decrease in current (24). Application of 100 μM Gd^{3+} activated doubly rectifying currents that were blocked by the TRPC5 inhibitor ML204 but did not decrease in magnitude over time (Fig. 1, *D* and *E*) (25). Incubation with 20 μM wortmannin decreased the peak Gd^{3+}-elicited currents by 74.16 ± 0.75% compared with untreated control cells (Fig. 1, *D*–*F*). Taken together, the results of Figure 1 implicate multiple roles for PIP_2 in the activation and inhibition of TRPC5 channels by both independent gating mechanisms by either Gq signaling or lanthanide stimulation.

PMA-mediated inhibition weakens channel–PIP_2 interactions

The spontaneous decrease in TRPC5 current observed after activation by CCh is proposed to be mediated by subsequent PKC-mediated phosphorylation of the channel (19). The two key molecules of interest in the desensitization pathway are the PKC enzymes, which induce desensitization by phosphorylation, and PIP_2, which opposes desensitization. To control the kinetics of TRPC5 current inhibition, we used optogenetic activation of 5' phosphatase to dephosphorylate PIP_2 in cells illuminated by 460 nm (blue) light. Briefly, blue light induces dimerization between two plant proteins, cryptochrome 2 (CRY2) and the transcription factor cryptochrome-interacting basic-helix-loop-helix N-terminal fragment (CIBN), to control

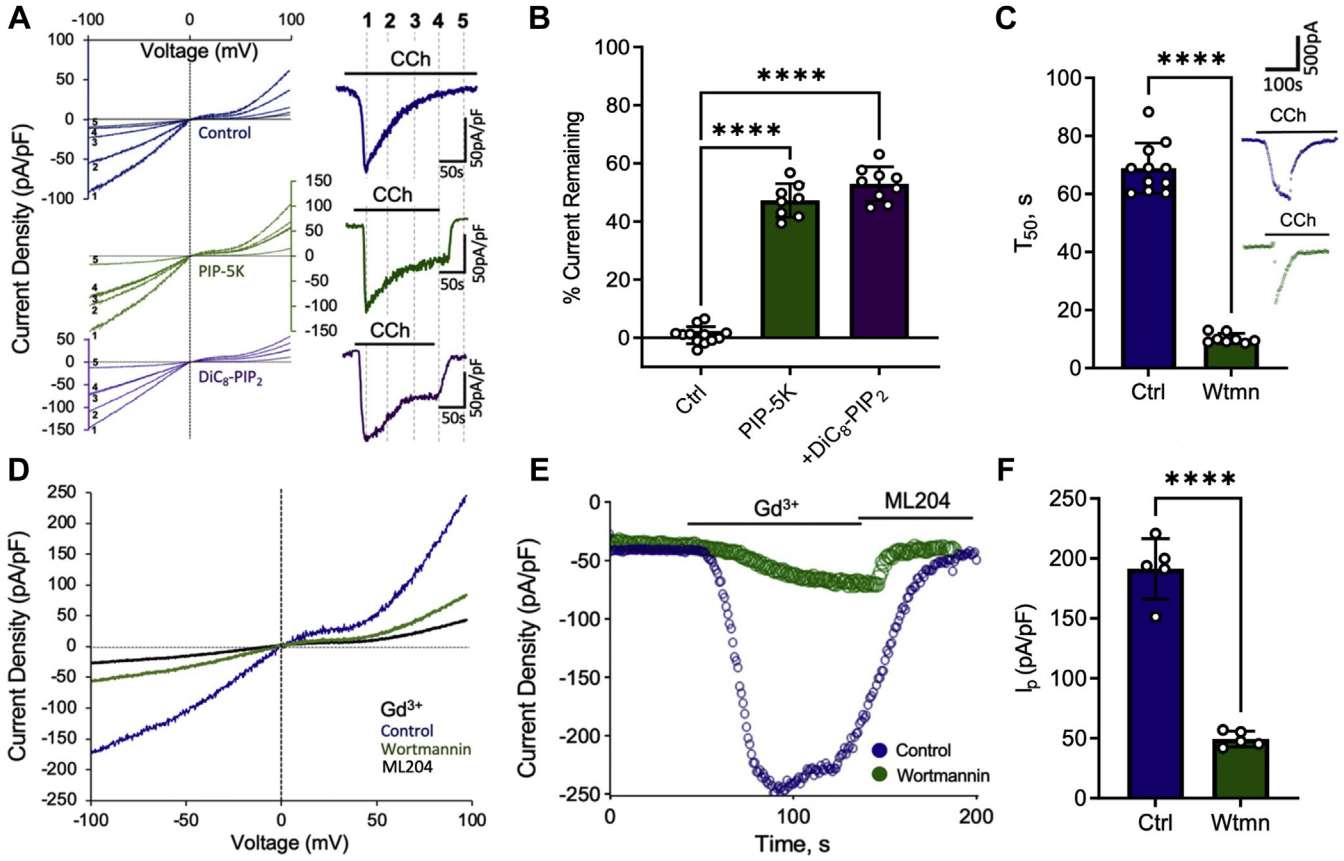

Figure 1. PIP_2 implicated in PKC-mediated desensitization and promotion of Gd^{3+}-activated TRPC5 currents. *A*, *left*, example current density and voltage relationships for HEK293T cells expressing mTRPC5–GFP. Currents were evoked by a ramp from −100 mV to 100 mV followed by application of 100 μM CCh. Cells were studied under control conditions (*blue*) or with PIP-5K coexpression (*green*) or with 200 μM diC_8–PIP_2 in the pipette (*purple*). The spontaneous decrease in current is illustrated by sweeps labeled 1 to 5, which correspond to 50-s intervals, as illustrated on the exemplar time courses (*right*). *B*, the mean of percentage current remaining during 100 μM CCh treatment in control HEK293T cells expressing mTRPC5–GFP (n = 12, 0.89 ± 2.948), with overexpression of PIP-5K (n = 9, 47.07 ± 5.78) and with diC_8–PIP_2 in the pipette (n = 10, 52.32 ± 5.89). *C*, the bar graph of time taken from peak to 50% current decay (T_{50}) of control HEK293T cells expressing mTRPC5–GFP (n = 11, 68.82 ± 8.681) and after treatment with 20 μM wortmannin for 1 h (n = 9, 10.23 ± 1.722); inset: representative whole-cell patch-clamp recordings in each condition of HEK293T cells expressing TRPC5–GFP activated by 100 μM CCh. *D*, current density voltage curves of the ±100 mV ramp of ML204-sensitive currents activated by 100 μM Gd^{3+} activation in TRPC5–GFP expressing HEK293T cells (control) and after 1 h treatment with 20 μM wortmannin. *E*, representative whole-cell current density (pA/pF) curves observed in HEK293T cells overexpressing mTRPC5–GFP activated with 100 μM $GdCl_3$ and upon 20 μM wortmannin treatment for 1 h. *F*, the bar graph of Ip (peak current density-pA/pF) of control HEK293T cells expressing TRPC5–GFP (n = 5, 191 ± 25.23) and cells treated with wortmannin (n = 5,49.35 ± 6.5). Values reported as mean ± SD, *p*-values established using Student's *t* test, $^{****}p < 0.0001$. CCh, carbachol; diC_8–PIP_2, dioctanoyl-glycerol-PIP_2; PIP-5K, phosphatidylinositol 4-phosphate 5 kinase; TRPC5, transient receptor potential canonical type 5.

the plasma membrane PIP_2 levels rapidly, locally, and reversibly. The 5'-phosphatase domain of OCRL (5'-ptaseOCRL), which acts on $PI(4,5)P_2$ and $PI(3,4,5)P_3$, is fused to the photolyase homology region domain of CRY2 (26). Stimulation of CRY2 with blue light binds CIBN, resulting in nearly instantaneous recruitment of 5'-ptaseOCRL to the plasma membrane and causing rapid $PI(4,5)P_2$ dephosphorylation to PI(4)P (26). We expressed the TRPC5 channel and light-activated CRY2–5'-ptaseOCRL and CIBN–CAAX–GFP proteins in HEK-293T cells to perform the blue light–activated phosphatase experiment in the whole-cell mode of the patch-clamp technique. Gd^{3+}-activated inward currents were allowed to stabilize before a blue light (460 nm, shown by the blue panels) was shone to activate the inositol 5'-phosphatase and deplete membrane PIP_2 until the current declined and reached a steady state (Fig. 2*A*).

Next, to examine the effect of PKC-mediated inhibition of the channel without causing a concurrent hydrolysis of PIP_2, PKC was activated using 100 nM phorbol 12-myristate-13-acetate (PMA) (Fig. 2*B*). To assess the role of PIP_2 on the PKC effect, we increased intracellular PIP_2 levels using diC_8–PIP_2 in the pipette (Fig. 2*B*). We observed that inclusion of diC_8–PIP_2 in the pipette solution decreased the rate and extent of desensitization induced by PMA (Fig. 2, *E* and *F*). This emphasizes the significance of channel–PIP_2 interaction strength on the inhibition of channel by PKC-mediated phosphorylation. We observed that selective dephosphorylation of PIP_2 (blue light phosphatase assay) or activation of PKC enzymes using the drug PMA, individually inhibit approximately 50% of the channel current, respectively (Fig. 2, *A* and *B*). Next, we probed the effect of PKC-mediated effects on the strength of channel–PIP_2 interaction by comparing the kinetics of inhibition due to dephosphorylation of PIP_2 before and after the channel was treated with PMA. The 5'-ptaseOCRL system has been used effectively to compare the influence of different channel modulators on the strength of

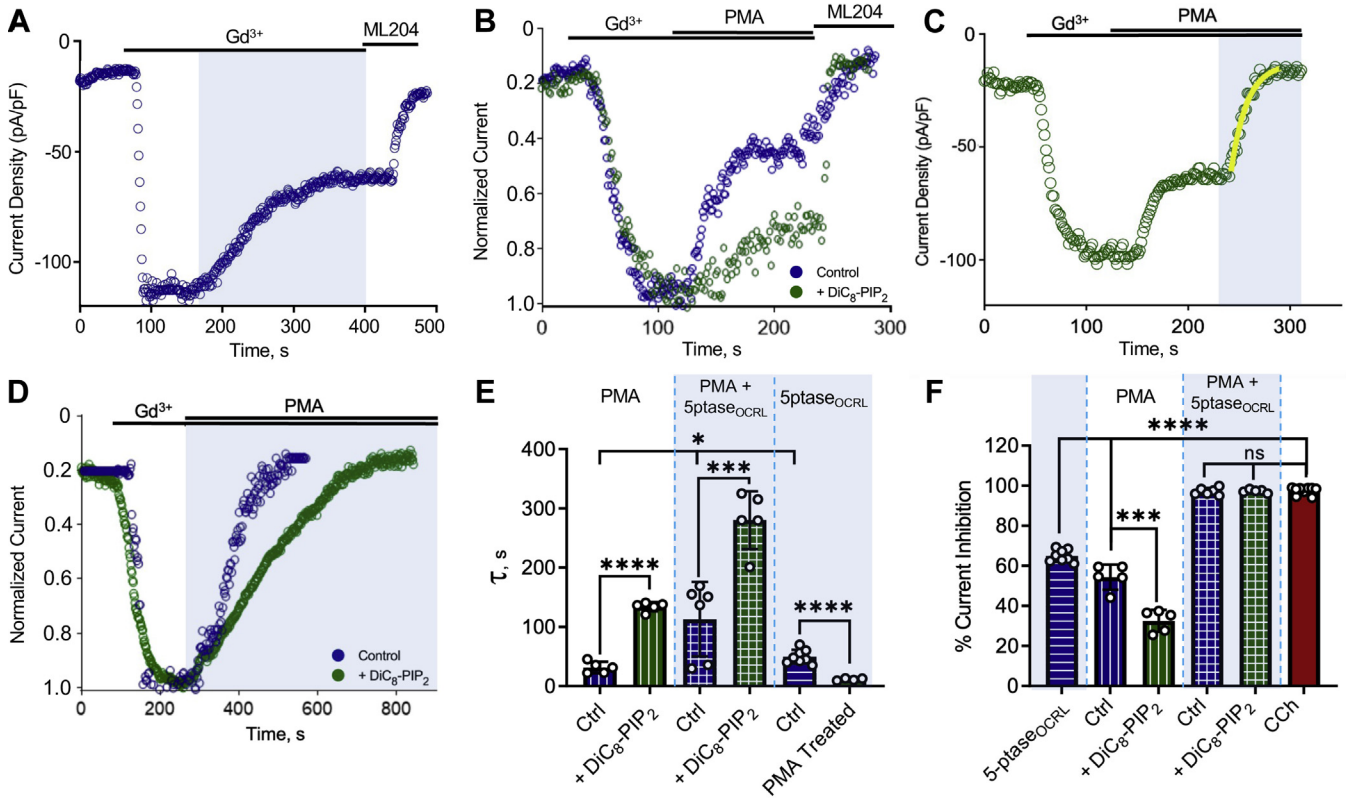

Figure 2. TRPC5 current inhibition by PKC-mediated phosphorylation and/or PIP_2 dephosphorylation reveals an underlying decrease in channel–PIP_2 interactions. *A*, whole-cell patch clamp recording of HEK293T cells expressing TRPC5–GFP, light-activated CRY2–5′PTASE$_{OCRL}$, and CIBN–CAAX–GFP (see Experimental procedures); inward current activated by 100 μM $GdCl_3$ with channel current decrease in response to light-activated metabolism of PIP_2 and remaining current blocked by 3 μM ML204. *B*, inhibition observed by PKC activator PMA without/with 200 μM diC_8–PIP_2 in the pipette. *C*, HEK-293T cells expressing TRPC5–GFP, CRY2–5′ptase, and CIBN–CAAX–GFP were activated using 100 μM $GdCl_3$; 200 nM PMA was applied to activate PKC enzymes followed by blue-light exposure. *D*, inhibition observed by simultaneous application of PKC activator PMA and activation of light-activated inositol phosphatase without/with 200 μM diC_8–PIP_2 in the pipette. *E*, the bar graph of the mean decay constant ± SD of PMA-mediated inhibition alone (n = 5, 31.44 ± 9.62) and with diC_8–PIP_2 (n = 5, 133.95 ± 7.766), simultaneous PMA and 5′-ptase$_{OCRL}$–mediated inhibition (n = 6, 112.97 ± 62.87) and with diC_8–PIP_2 (n = 5, 280.33 ± 48.71), and 5′-ptase$_{OCRL}$-mediated inhibition alone (n = 8, 52.57 ± 11.59) and after PMA treatment (n = 5, 11.43 ± 1.834). *F*, the bar graph summary of the mean percentage current inhibition ± SD by 5′-ptase$_{OCRL}$ (n = 8, 65.18 ± 3.046), PMA-mediated inhibition alone (n = 5, 54.4 ± 7.23), and with diC_8–PIP_2 (n = 5, 32.47 ± 6.04), simultaneous PMA and 5′-ptase$_{OCRL}$-mediated inhibition (n = 6, 97.51 ± 2.397) and with diC_8–PIP_2 (n = 5, 96.87 ± 0.8152), and when activated using 100 μM CCh (n = 12, 97.61 ± 2.32). Values reported as mean ± SD, *p*-values established using Students' *t* test, comparison with experimental control (#); *$p < 0.05$, ***$p < 0.001$, ****$p < 0.0001$. CCh, carbachol; CRY2, cryptochrome 2; diC_8–PIP_2, dioctanoyl-glycerol-PIP_2; PMA, phorbol 12-myristate-13-acetate; TRPC5, transient receptor potential canonical type 5.

channel–PIP_2 interactions (27). After the PMA-induced inhibition of TRPC5 currents reached a steady state (Fig. 2*C*), blue-light illumination yielded faster inhibition kinetics, suggesting that the PKC-mediated phosphorylation decreases channel–PIP_2 interactions (Fig. 2, *A*, *C* and *E* 5′-ptaseOCRL).

To test whether the complete current inhibition observed during PLC activation (see Fig. 1*A*) could be mimicked by simultaneous PIP_2 hydrolysis and PKC-mediated effects, the Gd^{3+}-activated channel was simultaneously treated with the PKC activator PMA and blue light to cause dephosphorylation of PIP_2. This resulted in a complete inhibition (Fig. 2, *D* and *F*) of channel currents similar to that observed in the Gq-activated system (Fig. 1*A*), suggesting that PKC activation and PIP_2 hydrolysis are both involved to cause complete channel inhibition when TRPC5 channels are activated by the Gq receptor signaling pathway. Next, we determined the effect of increased levels of intracellular PIP_2 by repeating the same experiment in cells studied with 200 μM diC_8–PIP_2 in the recording pipette. Elevated levels of PIP_2, and thus increased channel–PIP_2 interactions, decreased the rate of channel inhibition by simultaneous PIP_2 dephosphorylation and PKC activation (Fig. 2, *D* and *E*) but did not affect the extent of inhibition (Fig. 2, *D* and *F*). Given these results, we conclude that the rate of desensitization of TRPC5 channels by PKC is inversely affected by intracellular PIP_2 levels.

*1-oleoyl-2-acetyl-*sn*-glycerol strengthens TRPC5 channel–PIP_2 interactions to stimulate channel activity*

The T972A TRPC5 mutant is PKC-insensitive, abolishing the desensitization observed on Gq-mediated activation of the channel and enabling direct activation by 1-oleoyl-2-acetyl-*sn*-glycerol (OAG) (2, 17). Because our experiments thus far suggested that PKC-mediated phosphorylation is dependent on channel–PIP_2 interactions, we investigated further whether the PKC-insensitive mutant channel differs from the WT channel in its interaction with PIP_2. As previously shown, the PKC-insensitive TRPC5–T972A mutant

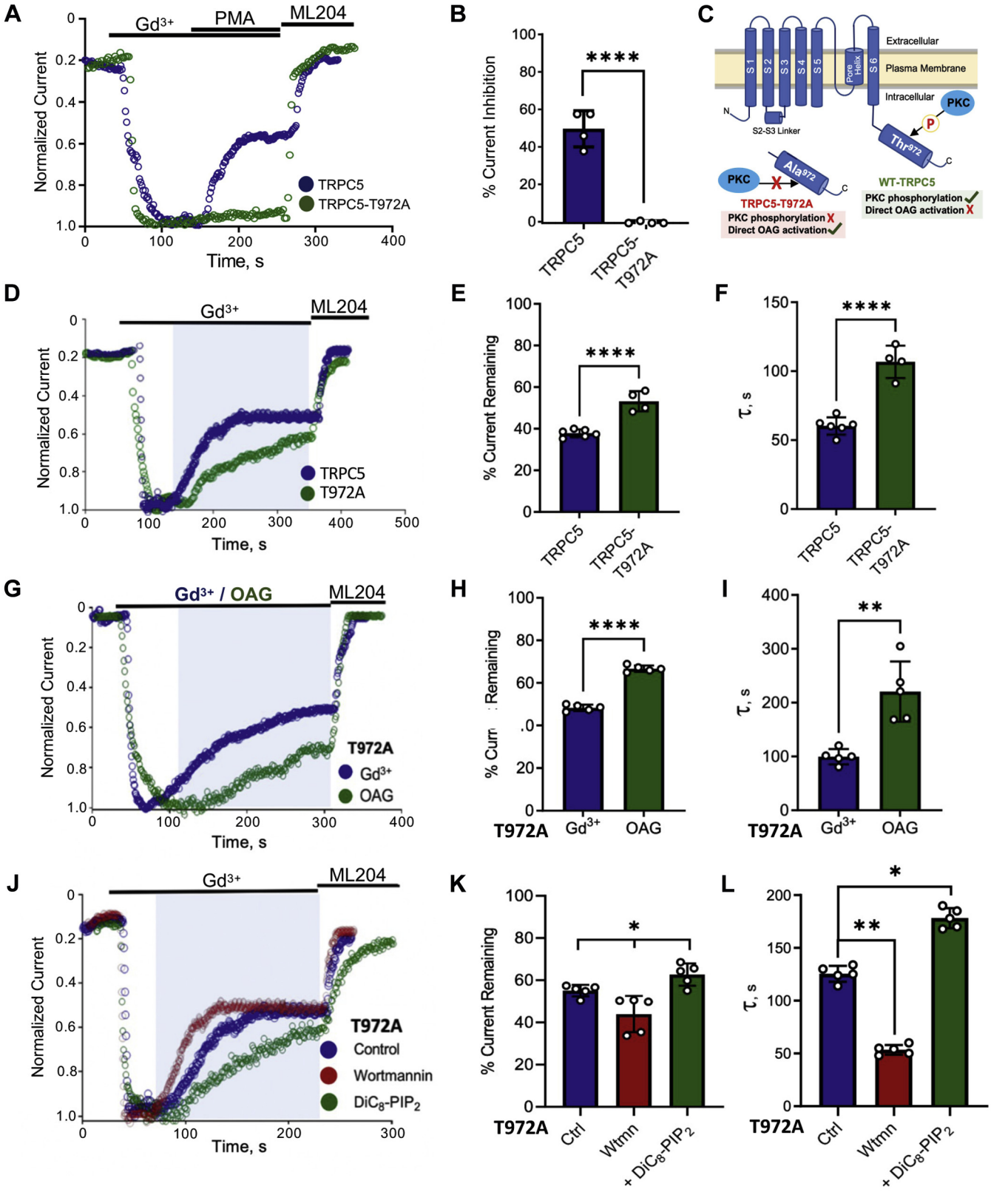

Figure 3. OAG-mediated activation of TRPC5 channels shows enhanced channel–PIP_2 interaction strength. *A*, HEK-293T cells expressing TRPC5–GFP/TRPC5–T972A–GFP were activated using 100 μM $GdCl_3$, and effect of 200 nM PMA was observed. *B*, the bar graph summary of the mean percentage current inhibition by PMA in WT TRPC5 (n = 4, 50.18 ± 9.87) and PKC-insensitive TRPC5–T972A mutant (n =4, 0.75 ± 0.96). *C*, cartoon depicting the differences between the WT and PKC-insensitive TRPC5–T972A mutant channels. *D*, HEK-293T cells expressing TRPC5–GFP/TRPC5–T972A–GFP, CRY2–5′ptase, and CIBN–CAAX–GFP were activated using 100 μM $GdCl_3$ and the effect of blue-light exposure was observed. *E*, the bar graph summary of the mean percentage current remaining ± SD (in panel *D*) in WT TRPC5 (n = 6, 37.83 ± 1.8392) and PKC-insensitive TRPC5–T972A mutant (n = 5, 53.175 ± 4.39). *F*, the bar graph of the mean decay constant of inhibition ± SD (in panel *D*) for TRPC5 (n = 6, 60.27 ± 9.79) for mTRPC5–T972A (n = 4, 106.67 ± 14.42). *G*, HEK-293T cells expressing TRPC5–T972A–GFP, CRY2–5′ptase, and CIBN–CAAX–GFP were activated using saturated concentration of Gd^{3+} (150 μM) or OAG (200 μM), and

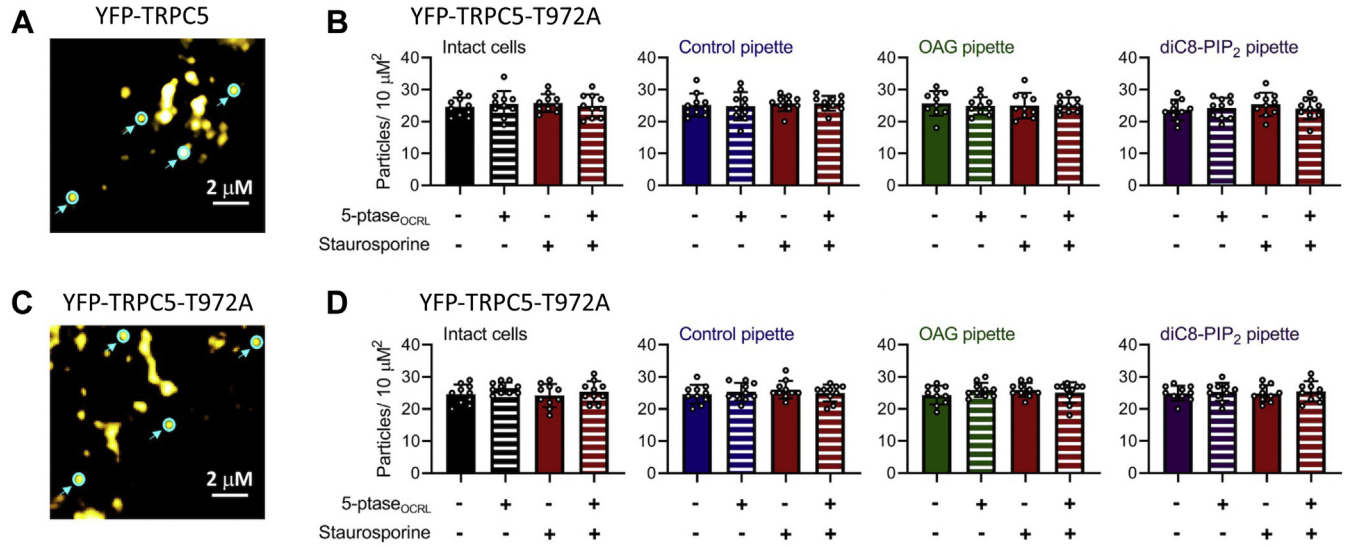

Figure 4. Regulation by OAG or PIP_2 does not alter the surface density of YFP–TRPC5 channels. YFP-tagged mTRPC5 or mTRPC5–T972A channels were expressed in HEK293T cells and studied by patch clamp TIRF. The number of fluorescent particles was determined 200 s after whole-cell mode was established to allow dialysis of the cells with the control solution (*blue*), 200 μM OAG (*green*) or 200 μM diC8–PIP_2 (*purple*). Cells were studied with or without optogenetic activation of 5′-ptaseOCRL (*white stripped bars*) or after incubation with 1 μM staurosporine (*red*). Bar graphs represent particle density as the mean ± SD number of fluorescent particles in the TIRF field in 3 to 6 random 10 × 10 μm squares per cell and from 4 to 6 cells per group. *A*, TIRF image showing YFP-tagged WT mTRPC5 channels at the cell surface. Four example particles corresponding to single TRPC5 channels are highlighted in *cyan*. *B*, the bar graphs summarizing the density of fluorescent particles indicating no change from control values under any of the conditions studied. *C*, TIRF image showing YFP-tagged mTRPC5–T972A channels at the cell surface. Four example particles corresponding to single TRPC5 channels are highlighted in *cyan*. *D*, the bar graphs summarizing the density of fluorescent particles indicating no change from control values under any of the conditions studied. *V*alues reported as mean ± SD, p-values established using Students' *t* test. diC_8–PIP_2, dioctanoyl-glycerol-PIP_2; TRPC5, transient receptor potential canonical type 5.

was unaffected by PMA application (Fig. 3, *A* and *B*). This mutant simplifies the experimental design by removing inhibition by PKC phosphorylation and allowing direct activation by DAG (2) (Fig. 3*C*). We used 100 μM $GdCl_3$ to activate the WT and T972A mutant channels to bypass the activation of the PLC pathway and assess channel–PIP_2 strength by exposure to blue light (Fig. 3*D*). The mutant channel exhibited a significantly less and slower inhibition (Fig. 3, *D–F*) than the WT channel, indicating a stronger channel–PIP_2 interaction than the WT. This result suggested the occurrence of basal PKC-dependent phosphorylation under unstimulated conditions. From this observation, we can conclude that the PKC-insensitive T972A mutant channel has stronger channel–PIP_2 interactions than the WT channel. The TRPC5 channel is thought to be activated by DAG, which is endogenously produced through hydrolysis of PIP_2 by PLC enzymes. As shown previously by Storch *et al.*, (2) the channel can be rendered sensitive to direct activation by OAG upon inhibition of PKC enzymes or upon mutation of the PKC phosphorylation site T972 to alanine. Thus, to understand the mechanism by which DAG is activating the channel and whether it occurs through modulating the channel's interaction with the remaining nonhydrolyzed PIP_2, we used a saturating concentration of OAG (200 μM) to activate the mutant TRPC5–T972A channel and compared its kinetics of inhibition upon blue light–induced PIP_2 dephosphorylation with that of a saturating concentration of Gd^{3+} (150 μM). T972A channels activated by OAG showed a less and slower inhibition upon dephosphorylation of PIP_2 than those activated by Gd^{3+} (Fig. 3, *G–I*), indicating that OAG activation is characterized by stronger interactions of the channel with PIP_2. To further look into the effect of PIP_2 levels on OAG-activated currents with and without the action of 5′-ptase, we depleted PIP_2 levels using wortmannin or increased intracellular PIP_2 levels by including diC_8–PIP_2 in the pipette solution (Fig. 3, *J–L*). We observed that in T972A channels upon wortmannin incubation, the peak current density of OAG-activated currents was significantly smaller than control (data not shown) or 200 μM PIP_2 in the pipette solution. Interestingly, these varied PIP_2 levels that affect channel–PIP_2 interaction strength also affected the rate of inhibition of OAG-activated currents upon dephosphorylation of the membrane PIP_2 using the blue light–

the effect of blue-light exposure was observed. *H*, the bar graph summary of the mean percentage current remaining ± SD (in panel *G*) in TRPC5–T972A upon activation by Gd^{3+} (n = 5, 48.32 ± 1.45) and OAG (n = 5, 66.7 ± 1.51). *I*, the bar graph of the mean decay constant of inhibition ± SD (in panel *G*) when activated by 150 μM Gd^{3+} (n = 5, 99.55 ± 14.11) and 200 μM of OAG (n = 5, 220.5 ± 56.03). *J*, HEK-293T cells expressing TRPC5–T972A–GFP, CRY2–5′ptase, and CIBN–CAAX–GFP were activated using 100 μM OAG (control) and incubated in 20 μM wortmannin for 1 h and 200 μM diC_8–PIP_2 in the pipette. *K*, the bar graph summary of the mean percentage current remaining ± SD (in panel *J*) in TRPC5–T972A upon activation by OAG (n = 5, 54.84 ± 7.51), with wortmannin (n =5, 43.94 ± 8.6) and diC_8–PIP_2 (n = 5, 62.64 ± 5.3). *L*, the bar graph of the mean decay constant of inhibition ± SD (in panel *J*) for control (n = 5, 125.5 ± 7.5), with wortmannin (n = 5, 53.25 ± 4.65) and with diC_8–PIP_2 (n = 5, 178.25 ± 9.45). Values reported as mean ± SD, *p*-values established using Students' *t* test, $*p < 0.05$, $**p < 0.01$, $****p < 0.0001$. CRY2, cryptochrome 2; diC_8–PIP_2, dioctanoyl-glycerol-PIP_2; PMA, phorbol 12-myristate-13-acetate; TRPC5, transient receptor potential canonical type 5.

activated phosphatase assay. This indicated that the activation of the channel by DAG, similar to channel desensitization by PKC (Fig. 2), is dependent on the channel–PIP_2 interaction strength.

The surface density of TRPC5 channels is not regulated by PIP_2 or OAG

Yellow fluorescent protein (YFP)-tagged TRPC5–T972A channels also expressed readily in HEK293T cells at levels similar to WT channels (25 ± 1 particles per 10 μm^2; n = 12) in both intact cells (Fig. 4, *A* and *C*), or when cells were studied in total internal reflection fluorescence (TIRF)-patch mode with control solution, 200 μM OAG, or 200 μM diC8–PIP_2 included in the pipette (Fig. 4, *B* and *D*). Like WT YFP-TRPC5 channels, the number of YFP–TRPC5–T972A channels at the cell membrane was not altered by treating cells with staurosporine, or *via* activation of 5'-$ptase_{OCRL}$, irrespective of the solution in the patch pipette (Fig. 4, *B* and *D*). Together, these findings suggest that changes in the current density of TRPC5 channels observed after changes in the level of PIP_2, or after activation of PKC, result from the regulation of channel activity and not from modified trafficking of channels to or from the cell membrane.

PIP_2 prevents PKC-mediated desensitization and promotes OAG-mediated activation in endogenously expressed TRPC5 channels

Because TRPC5 channels are known to be highly expressed in the hippocampus, we utilized the hippocampal neuronal cell line HT-22 to study the channel in a native system (2). The HT-22 murine cell line expresses predominantly TRPC5 channels (1–3 orders of magnitude higher than other TRPC channels, ref. (2)). We assessed TRPC5 currents in these cells by using the selective inhibitor AC1903 (6). TRPC5 channel current was observed upon Gd^{3+}application (Fig. 5, *A* and *B*), and like in the HEK293T cell overexpression system, it was OAG insensitive (data not shown). To investigate the role of PIP_2 on PKC-mediated desensitization, we examined the rate and extent of inhibition *via* PMA with and without diC_8–PIP_2 in the patch pipette. In the presence of increased intracellular PIP_2, PKC-mediated inhibition was slower and less efficient (Fig. 5, *C* and *D*), similar to observations in the HEK293T overexpression system (Fig. 2*E*). Next, to confirm the dependency of DAG-mediated activation on PIP_2 levels, we first incubated the cells in 1 μM staurosporine to inhibit PKC. This made the channel sensitive to OAG activation

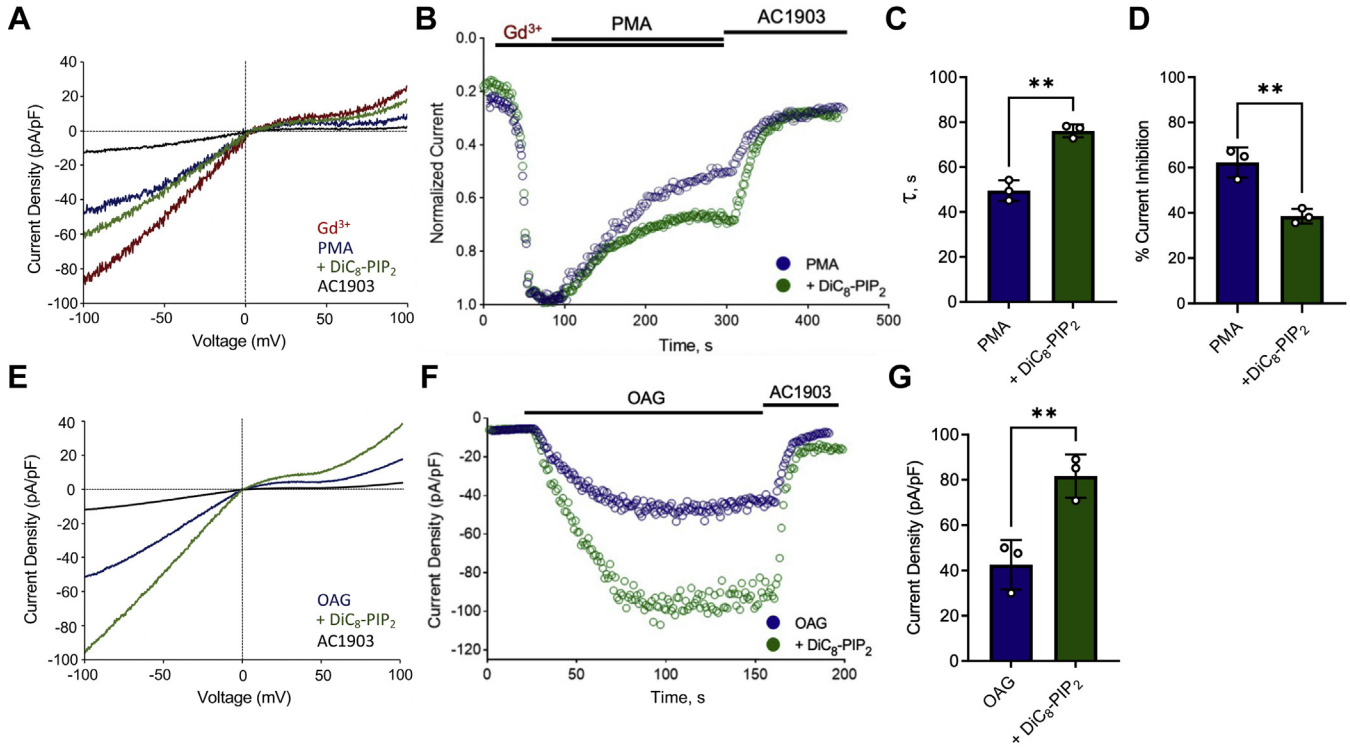

Figure 5. PIP_2 prevents PKC-mediated desensitization and promotes OAG-mediated activation in endogenously expressed TRPC5 channels. The experiments shown in this figure were carried out in HT-22 murine cells that predominantly express TRPC5 channels (2). *A*, current density voltage curves of the ± 100 mV ramp of 100 μM Gd^{3+}, PMA inhibition with/without 200 μM diC_8–PIP_2 in the pipette and inhibition with 100 μM AC1903 (a small-molecule selective inhibitor of TRPC5). *B*, representative whole-cell recording of PMA-mediated inhibition of Gd^{3+} with/without 200 μM diC_8–PIP_2. *C*, the bar graph summary of the mean decay constant of inhibition observed with PMA (control n = 3, 49.5 ± 4.55) and with 200 μM diC_8–PIP_2 (n = 3, 76 ± 2.87). *D*, the bar graph summary of mean percentage current inhibited ± SD with PMA (control n = 3, 62.26 ± 6.37) and with 200 μM diC_8–PIP_2 (n = 3, 38.8 ± 3.23). *E*, current density voltage curves of the ±100 mV ramp in HT-22 cells treated with 1 μM staurosporine for 30 min, of 100 μM OAG activation with/without 200 μM diC_8–PIP_2 in the pipette, and inhibition with 100 μM AC1903. *F*, representative whole-cell recording of 100 μM OAG-activated currents after treatment with 1 μM staurosporine for 30 min, with/without 200 μM diC_8–PIP_2. *G*, the bar graph summary of mean peak current density ± SD observed with 100 μM OAG (control n = 3, 42.5 ± 6.305) and with 200 μM diC_8–PIP_2 (n = 3, 81.6 ± 5.51). Values reported as mean ± SD, p-values established using Students' *t*-test $^{**}p < 0.01$. diC_8–PIP_2, dioctanoyl-glycerol-PIP_2; PMA, phorbol 12-myristate-13-acetate; TRPC5, transient receptor potential canonical type 5.

and produced further current stimulation by increased intracellular PIP_2 levels (Fig. 5, *E–G*). Having diC_8–PIP_2 in the patch pipette gave higher peak currents than control, indicating that PIP_2 contributes to a higher OAG-mediated channel activity. Altogether, these results indicate that PIP_2 regulation of endogenous TRPC5 channels mirrors its effect in heterologously expressed channels.

Discussion

Until now, the role of PIP_2 in the mechanism that regulates TRPC5 channel activity after stimulation of $G_{q/11}$-coupled receptors has remained largely elusive. Although there is evidence that TRPC5 channels become DAG sensitive upon PLC-mediated hydrolysis of PIP_2, the specific role of PIP_2 in channel activation or inhibition had not been probed (2). In this study, we show that TRPC5 channels are functionally coupled to PIP_2 and that DAG activation as well as PKC-mediated inhibition of the channel, through phosphorylation at T972, involve modulation of channel–PIP_2 interactions. Our findings consolidate and synthesize prior seemingly discrepant results on the role of PIP_2 into a single, coherent model.

We found that in trivalent ion-mediated channel gating, Gd^{3+} strengthens channel–PIP_2 interaction to cause submaximal channel activation (see model in Fig. 6, strength 4 of 5 or 4/5). PKC-mediated phosphorylation of the channel (PMA treatment) weakens channel–PIP_2 interactions and causes partial inhibition (strength 3/5). Similarly, PIP_2 depletion (5'-phosphatase) inhibits activity partially because of the high-affinity of the channel for PIP_2 that protects the channel from losing all of its interacting PIP_2 molecules in the Gd^{3+} activated state (7). A combination of PIP_2 depletion and PKC-mediated channel phosphorylation fully inhibits currents below basal levels, as the channel is now less able to hold on to its interacting PIP_2 molecules (strength 1/5). Trivalent ion gating of TRPC5 channels is more straight forward than Gq-mediated gating as activation and inhibition can be controlled separately and simultaneously.

$G_{q/11}$-mediated gating is more complex because of the fact that all four components, PIP_2 depletion, DAG production and channel activation, DAG-mediated activation of PKC, and channel inhibition cannot be readily separated as with Gd^{3+} gating. The activating molecule DAG interacts with the intracellular side of the channel to strengthen channel–PIP_2 interactions and yield maximal activation (strength 5/5), while protecting the channel from losing its PIP_2 despite the ongoing PLC-meditated hydrolysis. For DAG to stimulate activity, the dominating inhibitory PKC phosphorylation needs to be abrogated. The obligate activation of PKC by the generated DAG molecules phosphorylates the channel at T972, weakening channel–PIP_2 interactions (strength 1/5) and making the channel activation transient, as DAG-mediated activation is followed by complete inhibition of activity. Desensitization

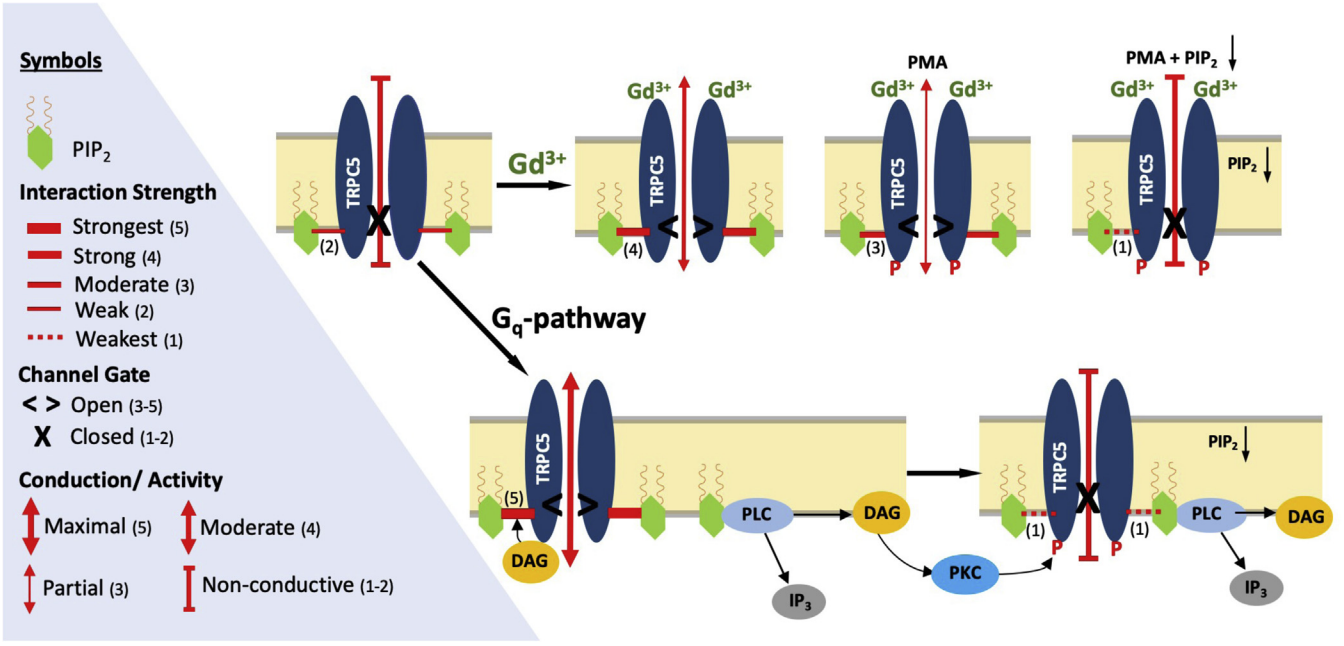

Figure 6. Cartoon model of the dependency of TRPC5 channel on PIP_2 to account for stimulation and inhibition of channel activity by independent gating mechanisms. Trivalent cation-mediated control of TRPC5 activity: Trivalent cation activation mediated by Gd^{3+} allosterically strengthens channel interactions with PIP_2, strongly enough to cause partial activation. PMA treatment alone (PKC-mediated phosphorylation but not PIP_2 depletion) weakens channel–PIP_2 interaction strength and causes partial inhibition of channel currents. Similarly, depletion of intracellular PIP_2 levels (using either wortmannin or 5'-phosphatase) alone (PIP_2 depletion but not PKC-mediated phosphorylation) does not strip the channel completely of its PIP_2 causing partial inhibition of activity. The combination of PMA treatment and PIP_2 depletion strips the channel from its PIP_2 severely enough to cause full inhibition. Gq-mediated control of TRPC5 activity: upon Gq-receptor activation, PLC hydrolyzes PIP_2 to IP_3 and DAG. DAG allosterically enhances stronger channel interactions with PIP_2, activating the channel maximally. PIP_2 depletion (such as by dephosphorylation of PIP_2) alone (without PKC-mediated phosphorylation as in T972A) causes partial inhibition. The ensuing DAG activation of PKC causes channel phosphorylation at T972, which allosterically weakens channel–PIP_2 interactions enough that adds up to the PIP_2 depletion causing full inhibition of the current. IP_3, inositol 1,4,5-triphosphate; PLC, phospholipase C; PMA, phorbol 12-myristate-13-acetate; TRPC5, transient receptor potential canonical type 5.

ensues as the hydrolyzed PIP_2 needs to be resynthesized and protein phosphatases need to dephosphorylate the channel at T972 to render it activatable again by DAG. Our model proposes that although Gd^{3+} and DAG use different pathways to activate TRPC5 channels, they converge at the level of channel–PIP_2 interactions, which they control allosterically. Thus, in this model, it is PIP_2 and its interactions with TRPC5 that should be deemed essential for channel activation and inhibition.

TRPC3/6/7 channels are highly sensitive to PLC-mediated PIP_2 depletion, which correlates with the spontaneous inhibition of DAG-activated currents observed (28). TRPC4/5 channels are uniquely regulated by C-terminal interactions with NHERF proteins, where in the NHERF-bound state, the channel is DAG insensitive (2). Our proposed model suggests that PIP_2 is significant for maximal channel activity and that a balance exists between PLC-mediated hydrolysis of PIP_2 to make DAG which activates all of the TRPC channels and the remaining PIP_2 molecules that are bound to the channel. When TRPC3-7 channels lose all of the bound PIP_2, due to PKC-mediated phosphorylation that weakens channel–PIP_2 interaction and the concurrent PIP_2 hydrolysis by PLC enzymes, channel currents are fully inhibited. We speculate that an interplay exists between phosphorylated channel subunits and PIP_2-bound subunits that lead to differences in activation and conduction in TRPC3-7 channels.

Previous studies performed to test the effect of PIP_2 depletion using the PI3K and PI4K inhibitor wortmannin showed that depleting PIP_2 had no effect on CCh-mediated currents, whereas increasing PIP_2 levels reduced the extent of CCh-mediated inhibition of TRPC5 channel currents (5, 19, 29). In an attempt to resolve these conflicting results, we incubated the cells with wortmannin to achieve the full effect and successfully deplete intracellular PIP_2 levels. Under these conditions, we observed that wortmannin increased the rate of CCh-mediated inhibition and reduced the peak of Gd^{3+}-activated currents. This conclusion was strengthened by the inability of increased PIP_2 levels to prevent complete current inhibition during simultaneous PKC and 5' phosphatase effect. This suggests that PKC phosphorylation is dominant and, together with PIP_2 depletion (PLC-mediated), results in irreversible inhibition of current that is unaffected by subsequent increases (diC_8–PIP_2) or decreases (by wortmannin) in PIP_2 levels, as previously shown (5, 19, 29).

Fundamentally, the PIP_2 dependency of several channels, including TRPC5, has been demonstrated in the inside-out patch configuration when, during patch excision, current rundown caused by a decrease in membrane PIP_2 levels can be reversed by addition of PIP_2 (8, 9). Trebak *et al.* established the role of an inhibitory factor that is associated with the channel in a PIP_2-dependent manner, which was later identified by Storch *et al.* to be the NHERF1/2 proteins (2, 5). However, the dependency of the affinity of the NHERF proteins for the channel on PIP_2 levels remains to be explored. The underlying question to address going forward is whether channel–PIP_2 binding physiologically accompanies NHERF protein binding and its inhibition of channel current. In addition, Trebak *et al.* (5) suggested a possible minor role for PI(4)P in the maintenance of TRPC5 currents. Our 5'-ptaseOCRL experiments do not directly address a possible minor role of the resulting PI(4)P on channel activity, a question that ought to be addressed in future work.

Altogether, we propose a model whereby channel–PIP_2 interactions are important for TRPC5 channel activation and for maintenance of channel activity, assigning a critical functional role to PIP_2 for this channel. We conclude that the dependence of channel activity on PIP_2 levels may be a characteristic of all TRPC channels.

The broader relevance of this work is underscored by the fact that TRPC5 inhibitors are now being tested in phase 2 studies in the clinic for the treatment of diseases caused by a leaky kidney filter, a direct consequence of the activation of TRPC5-mediated injury pathway in podocytes. A deeper understanding of the activation mechanisms of TRPC5 may enable the development of more selective and precise molecules to block TRPC5 channel activity in podocytes. Diseases driven by kidney filter damage, otherwise known as proteinuric or glomerular kidney diseases, account for the majority of the 850 million patients suffering from progressive kidney diseases worldwide. Therefore, our detailed studies can illuminate new therapeutic opportunities for targeted therapies for a group of diseases for which there is currently a great unmet need.

Experimental procedures

Cell culture

Human embryonic kidney (HEK293T) cells and hippocampal HT-22 cells were acquired from American type culture collection and maintained in Dulbecco's modified Eagle's medium (Sigma-Aldrich) supplemented with 100 units/ml penicillin, 100 μg/ml streptomycin, and 10% (vol/vol) fetal bovine serum. All cells were held at 37 °C in a humified atmosphere with 5% CO_2.

Materials

OAG was purchased from Cayman Chemical, diC8–PIP2 was from Echelon Biosciences, and ML204 and AC1903 were received from Dr Corey Hopkins' Lab (University of Nebraska). PMA was purchased from LC labs, and Hepes was from Oakwood Chemical. All other materials were purchased from Sigma-Aldrich.

Molecular biology

Mouse TRPC5–GFP cDNA (NM_009428.2) constructs were used for whole-cell electrophysiology experiments. YFP was subcloned into the enhanced green fluorescent protein site/C-terminal end of the plasmid using respective restriction enzymes for TIRF experiments. Amino acid exchanges from Thr to Ala at position 972 in murine TRPC5 were introduced by site-directed mutagenesis using the QuikChange system (Stratagene). The cDNA constructs used in the present work were confirmed by Sanger sequencing (Macrogen). CIBN–CAAX–GFP and CRY2–5'-$ptase_{OCRL}$ were kind gifts from the

De Camilli lab (Yale). For TIRF experiments, the constructs were modified to remove existing fluorescent proteins.

Electrophysiological whole-cell measurements

HEK293T/HT-22 cells were seeded onto glass coverslips for whole-cell patch-clamp experiments. HEK293T cells were transfected with 2.5 μg of mTRPC5–GFP, 2.5 μg mTRPC5–T972A-GFP, 0.75 μg CIBN–CAAX–GFP, and 0.75 μg CRY2–5'ptase-mCherry for the respective experiments using polyethylenimine. TIRF experiments were performed on cells transfected with 1 μg of YFP–mTRPC5 or YFP–TRPC5–T972A plus or minus, 0.75 μg CIBN–CAAX–GFP, and 0.75 μg CRY2–5'ptase where indicated. All experiments were performed 18 to 24 h after transfection. The standard pipette solution for whole-cell patch-clamp contained, in millimolar, the following chemicals: 140 CsCl, 2 EGTA, 10 Hepes, 0.2 Na_3–GTP, and 2 $MgCl_2$. The bath solution contained, in millimolar, the following chemicals: 140 NaCl, 5 CsCl, 10 Hepes, 2 $MgCl_2$, 2 $CaCl_2$, and 10 glucose. Both solutions were adjusted to pH 7.4 with NaOH. The patch pipettes were made using a two-step protocol (Sutter Instruments) and had a resistance between 5 and 8 MΩ. Once the whole-cell configuration was achieved, cells were clamped at a holding potential of −60 mV using a patch-clamp amplifier (Tecella), controlled by WinWCP software (University of Strathclyde, UK). Currents were studied using a voltage ramp stimulation from −100 mV to +100 mV applied every 1 s. Data were low-pass filtered at 2 kHz, digitized at 10 kHz, and analyzed using Clampfit (Molecular Devices). Liquid junction potentials were less than 3 MΩ and were not compensated for.

Total internal reflection microscopy

Single fluorescent YFP-tagged mTRPC5 or mTRPC5–T972A channels were identified and studied at the surface of live HEK293T cells by TIRF microscopy, as described previously (30). Cells were seeded to #1.5 glass coverslips, transfected as described above, and studied in the bath solution described above 18 to 24 h after transfection. The evanescent wave for TIRF was established and calibrated to 100 nm using micromirrors positioned below a high numerical aperture apochromat objective (60×, 1.5 NA; Olympus) mounted on an RM21 microscope frame (Mad City Labs) (31). YFP was excited by a 514-nm laser line (Coherent), and the emission was collected through a 540/30 nm bandpass filter (Chroma) using an sCMOS back-illuminated camera (Teledyne Photometrics) controlled by Micro-Manager freeware. Images were captured with a 200-ms exposure every 5 s. The surface density of single fluorescent channels was determined from 3 to 6 random 10 × 10 μm squares per cell (representing 100 × 100 pixels) and from 4 to 6 cells per group using the Analyze plugin in ImageJ. Intracellular application of OAG or PIP_2 was accomplished by dialyzing the cytoplasm *via* a patch pipette in whole-cell mode using the standard pipette solution described above. TIRF patch mode was achieved using a micromanipulator mounted on the stage of the microscope to position the pipette and development of whole-cell mode was monitored using a patch clamp amplifier (Tecella) controlled by WinWCP software (University of Strathclyde, UK). To allow for full dialysis, cells were studied 200 s after whole-cell mode was established. Optogenetic dephosphorylation of PIP_2 was performed in cells cotransfected with CRY2–5'-$ptase_{OCRL}$ and CIBN–CAAX (see *Molecular biology*) using 100-s illumination from a 445-nm laser line (Coherent).

Statistical analysis

All statistical analyses were carried out using Graphpad Prism software. Results are presented as the mean ± SD unless otherwise indicated. The comparisons were carried out using the Student's *t* test. $p < 0.05$ was considered statistically significant.

Data availability

All data are contained within the article.

Acknowledgments—We thank the members of D. E. L. and L. D. P. laboratories, Takeharu Kawano for help with molecular biology, Heikki Vaananen for technical support, Austin Baggetta for preparing and transfecting cells, and Corey Hopkins for providing us with ML204 and AC1903. We are grateful to Yiming Zhou, Juan Lorenzo Pablo, and James Pentikis for helpful discussions and Tibor Rohacs for critical feedback on the article.

Author contributions—M. N. and L. D. P. performed research and analyzed data. M. N., L. D. P., A. G., and D. E. L. designed research. M. N. and D. E. L. wrote the article.

Funding and additional information—The work was supported by Grants R01HL09549-23 to D. E. L., R01HL144615 to L. D. P., and R01DK095045 and R01DK099465 to A. G.

Conflict of interest—A. G. has a financial interest in Goldfinch Biopharma, which was reviewed and is managed by Brigham and Women's Hospital, Mass General Brigham (MGB), and the Broad Institute of MIT and Harvard in accordance with their conflict-of-interest policies. All other authors declare that they have no conflicts of interest with the contents of this article.

Abbreviations—The abbreviations used are: 5'-ptaseOCRL, 5'-phosphatase domain of OCRL; CCh, carbachol; CIBN, cryptochrome-interacting basic-helix-loop-helix N-terminal fragment; CRY2, cryptochrome 2; DAG, diacylglycerol; diC_8–PIP_2, dioctanoyl-glycerol-PIP_2; IP_3, inositol 1,4,5-triphosphate; NHERF, Na^+/H^+ exchanger regulatory factor; OAG, 1-oleoyl-2-acetyl-*sn*-glycerol; PIP-5K, phosphatidylinositol 4-phosphate 5 kinase; PLC, phospholipase C; PIP2, phosphatidylinositol 4,5-bisphosphate; PMA, phorbol 12-myristate-13-acetate; TIRF, total internal reflection fluorescence; TRPC5, transient receptor potential canonical type 5; YFP, yellow fluorescent protein.

References

1. Clapham, D. E. (2003) TRP channels as cellular sensors. *Nature* **426**, 517–524
2. Storch, U., Forst, A. L., Pardatscher, F., Erdogmus, S., Philipp, M., Gregoritza, M., y Schnitzler, M. M., and Gudermann, T. (2017) Dynamic NHERF interaction with TRPC4/5 proteins is required for channel gating by diacylglycerol. *Proc. Natl. Acad. Sci. U. S. A.* **114**, 37–46

3. Schaldecker, T., Kim, S., Tarabanis, C., Tian, D., Hakroush, S., Castonguay, P., Ahn, W., Wallentin, H., Heid, H., Hopkins, C. R., Lindsley, C. W., Riccio, A., Buvall, L., Weins, A., and Greka, A. (2013) Inhibition of the TRPC5 ion channel protects the kidney filter. *J. Clin. Invest.* **123**, 5298–5309
4. Bezzerides, V. J., Ramsey, I. S., Kotecha, S., Greka, A., and Clapham, D. E. (2004) Rapid vesicular translocation and insertion of TRP channels. *Nat. Cell Biol.* **6**, 709–720
5. Trebak, M., Lemonnier, L., DeHaven, W. I., Wedel, B. J., Bird, G. S., and Putney, J. W. (2009) Complex functions of phosphatidylinositol 4, 5-bisphosphate in regulation of TRPC5 cation channels. *Pflügers Arch.* **457**, 757–769
6. Zhou, Y., Castonguay, P., Sidhom, E. H., Clark, A. R., Dvela-Levitt, M., Kim, S., Sieber, J., Wieder, N., Jung, J. Y., Andreeva, S., Reichardt, J., Dubois, F., Hoffmann, S. C., Basgen, J. M., Montesinos, M. S., *et al*. (2017) A small-molecule inhibitor of TRPC5 ion channels suppresses progressive kidney disease in animal models. *Science* **358**, 1332–1336
7. Venkatachalam, K., Zheng, F., and Gill, D. L. (2003) Regulation of canonical transient receptor potential (TRPC) channel function by diacylglycerol and protein kinase C. *J. Biol. Chem.* **278**, 29031–29040
8. Hilgemann, D. W., and Ball, R. (1996) Regulation of cardiac Na^+, Ca^{2+} exchange and K_{ATP} potassium channels by PIP_2. *Science* **273**, 956–959
9. Logothetis, D. E., Petrou, V. I., Zhang, M., Mahajan, R., Meng, X. Y., Adney, S. K., Cui, M., and Baki, L. (2015) Phosphoinositide control of membrane protein function: A frontier led by studies on ion channels. *Annu. Rev. Physiol.* **77**, 81–104
10. Hansen, S. B., Tao, X., and MacKinnon, R. (2011) Structural basis of PIP 2 activation of the classical inward rectifier K+ channel Kir2.2. *Nature* **477**, 495–498
11. Whorton, M. R., and MacKinnon, R. (2011) Crystal structure of the mammalian GIRK2 K+ channel and gating regulation by G proteins, PIP2, and sodium. *Cell* **147**, 199–208
12. Whorton, M. R., and MacKinnon, R. (2013) X-ray structure of the mammalian GIRK2–βγ G-protein complex. *Nature* **498**, 190–197
13. Li, D., Jin, T., Gazgalis, D., Cui, M., and Logothetis, D. E. (2019) On the mechanism of GIRK2 channel gating by phosphatidylinositol bisphosphate, sodium, and the Gβγ dimer. *J. Biol. Chem.* **294**, 18934–18948
14. Duan, J., Li, J., Chen, G. L., Ge, Y., Liu, J., Xie, K., Peng, X., Zhou, W., Zhong, J., Zhang, Y., and Xu, J. (2019) Cryo-EM structure of TRPC5 at 2. 8-Å resolution reveals unique and conserved structural elements essential for channel function. *Sci. Adv.* **5**, eaaw7935
15. Chen, X., Li, W., Riley, A. M., Soliman, M., Chakraborty, S., Stamatkin, C. W., and Obukhov, A. G. (2017) Molecular determinants of the sensitivity to Gq/11-phospholipase C-dependent gating, Gd3+ potentiation, and Ca2+ permeability in the transient receptor potential canonical type 5 (TRPC5) channel. *J. Biol. Chem.* **292**, 898–911
16. Jung, S., Mühle, A., Schaefer, M., Strotmann, R., Schultz, G., and Plant, T. D. (2003) Lanthanides potentiate TRPC5 currents by an action at extracellular sites close to the pore mouth. *J. Biol. Chem.* **278**, 3562–3571
17. Semtner, M., Schaefer, M., Pinkenburg, O., and Plant, T. D. (2007) Potentiation of TRPC5 by protons. *J. Biol. Chem.* **282**, 33868–33878
18. Sharma, S., and Hopkins, C. R. (2019) Review of transient receptor potential canonical (TRPC5) channel modulators and diseases: Mini-perspective. *J. Med. Chem.* **62**, 7589–7602
19. Zhu, M. H., Chae, M., Kim, H. J., Lee, Y. M., Kim, M. J., Jin, N. G., Yang, D. K., So, I., and Kim, K. W. (2005) Desensitization of canonical transient receptor potential channel 5 by protein kinase C. *Am. J. Physiol. Cell Physiol.* **289**, 591–600
20. Kobrinsky, E., Mirshahi, T., Zhang, H., Jin, T., and Logothetis, D. E. (2000) Receptor-mediated hydrolysis of plasma membrane messenger PIP 2 leads to K+-current desensitization. *Nat. Cell Biol.* **2**, 507–514
21. Keselman, I., Fribourg, M., Felsenfeld, D. P., and Logothetis, D. E. (2007) Mechanism of PLC-mediated Kir3 current inhibition. *Channels* **1**, 113–123
22. Rohacs, T. (2014) Phosphoinositide regulation of TRP channels. *Handb Exp Pharmacol* **223**, 1143–1176
23. Atwood, B. K., Lopez, J., Wager-Miller, J., Mackie, K., and Straiker, A. (2011) Expression of G protein-coupled receptors and related proteins in HEK293, AtT20, BV2, and N18 cell lines as revealed by microarray analysis. *BMC Genomics* **12**, 1–14
24. Tang, Q. Y., Zhang, Z., Xia, J., Ren, D., and Logothetis, D. E. (2010) Phosphatidylinositol 4, 5-bisphosphate activates Slo3 currents and its hydrolysis underlies the epidermal growth factor-induced current inhibition. *J. Biol. Chem.* **285**, 19259–19266
25. Miller, M., Shi, J., Zhu, Y., Kustov, M., Tian, J. B., Stevens, A., Wu, M., Xu, J., Long, S., Yang, P., and Zholos, A. V. (2011) Identification of ML204, a novel potent antagonist that selectively modulates native TRPC4/C5 ion channels. *J. Biol. Chem.* **286**, 33436–33446
26. Idevall-Hagren, O., Dickson, E. J., Hille, B., Toomre, D. K., and De Camilli, P. (2012) Optogenetic control of phosphoinositide metabolism. *Proc. Natl. Acad. Sci. U. S. A.* **109**, 2316–2323
27. Xu, Y., Cantwell, L., Molosh, A. I., Plant, L. D., Gazgalis, D., Fitz, S. D., Dustrude, E. T., Yang, Y., Kawano, T., Garai, S., Noujaim, S. F., Shekhar, A., Logothetis, D. E., and Thakur, G. A. (2020) The small molecule GAT1508 activates brain-specific GIRK1/2 channel heteromers and facilitates conditioned fear extinction in rodents. *J. Biol. Chem.* **295**, 3614–3634
28. Itsuki, K., Imai, Y., Hase, H., Okamura, Y., Inoue, R., and Mori, M. X. (2014) PLC mediated PI (4, 5) P2 hydrolysis regulates activation and inactivation of TRPC6/7 channels. *J. Gen. Physiol.* **143**, 183–201
29. Kim, B. J., Kim, M. T., Jeon, J. H., Kim, S. J., and So, I. (2008) Involvement of phosphatidylinositol 4, 5-bisphosphate in the desensitization of canonical transient receptor potential 5. *Biol. Pharm. Bull.* **31**, 1733–1738
30. Plant, L. D., Xiong, D., Romero, J., Dai, H., and Goldstein, S. A. (2020) Hypoxia produces pro-arrhythmic late sodium current in cardiac myocytes by SUMOylation of NaV1. 5 channels. *Cell Rep.* **30**, 2225–2236.e4
31. Larson, J., Kirk, M., Drier, E. A., O'brien, W., MacKay, J. F., Friedman, L. J., and Hoskins, A. A. (2014) Design and construction of a multiwavelength, micromirror total internal reflectance fluorescence microscope. *Nat. Protoc.* **9**, 2317–2328

Mehek Ningoo is a PhD student at the Icahn School of Medicine at Mount Sinai pursuing her thesis work in the Fribourg Lab at the Translational Transplant Research Center. She studies the modulatory effects of type 1 interferon cytokine receptors in regulatory T cells and their impact on allograft survival. Mehek is leveraging biochemical signaling expertise acquired in the Logothetis lab at Northeastern University to study complex receptor interactions in immunology.